UCRL 2858

UNIVERSITY OF CALIFORNIA

Radiation Laboratory

PION PRODUCTION BY NEUTRONS ON HELIUM

TWO-WEEK LOAN COPY

This is a Library Circulating Copy which may be borrowed for two weeks. For a personal retention copy, call Tech. Info. Division, Ext. 5545

DISCLAIMER

This document was prepared as an account of work sponsored by the United States Government. While this document is believed to contain correct information, neither the United States Government nor any agency thereof, nor the Regents of the University of California, nor any of their employees, makes any warranty, express or implied, or assumes any legal responsibility for the accuracy, completeness, or usefulness of any information, apparatus, product, or process disclosed, or represents that its use would not infringe privately owned rights. Reference herein to any specific commercial product, process, or service by its trade name, trademark, manufacturer, or otherwise, does not necessarily constitute or imply its endorsement, recommendation, or favoring by the United States Government or any agency thereof, or the Regents of the University of California. The views and opinions of authors expressed herein do not necessarily state or reflect those of the United States Government or any agency thereof or the Regents of the University of California.

UCRL-2858
Unclassified Physics

UNIVERSITY OF CALIFORNIA
Radiation Laboratory
Berkeley, California

Contract No. W-7405-eng-48

PION PRODUCTION BY NEUTRONS ON HELIUM

Peter Hill Moulthrop
(Thesis)

January 31, 1955

Printed for the U.S. Atomic Energy Commission

PION PRODUCTION BY NEUTRONS ON HELIUM

Contents

Abstract 3
I Introduction 4
II Experimental Procedure
Cyclotron Run 6
The Cloud Chamber 9
III Measurements and Reduction of Observations
Detection and Measurement of Events 13
Identification of Particles 14
Errors 16
IV Results and Discussion
Branching Ratios and Fast Prongs 22
Angular Distribution 28
Energy Distribution 34
Energy Spectrum of Neutrons Producing Mesons . 34
Total Cross Section 34
Infrequent Events 35
V Acknowledgments 38
VI Appendices
Magnetic Field 39
Sample Pictures and Calculations 40
VII Bibliography 45

PION PRODUCTION BY NEUTRONS ON HELIUM

Peter Hill Moulthrop

Radiation Laboratory, Department of Physics,
University of California, Berkeley, California

January 31, 1955

ABSTRACT

A helium-filled 36-atmosphere diffusion cloud chamber in a pulsed 21,000-gauss magnetic field was operated in the 300-Mev neutron beam of the 184-inch cyclotron. Two hundred and ninety five negative pions were found, with associated prongs as indicated in the table.

Partial Cross Sections for Negative Pion Production in 300-Mev n-α Collisions

Reaction	Percent
$n + \alpha \rightarrow \alpha + p + \pi^-$	5.7 ± 1.4
$n + \alpha \rightarrow p + He^3 + n + \pi^-$	32.0 ± 3.3
$n + \alpha \rightarrow \alpha + p + \pi^-$ or $p + He^3 + n + \pi^-$	4.6 ± 1.2
$n + \alpha \rightarrow d + He^3 + \pi^-$	30.4 ± 3.2
$n + \alpha \rightarrow p + p + d + n + \pi^-$	15.4 ± 2.3
$n + \alpha \rightarrow d + d + p + \pi^-$	6.2 ± 1.5
$n + \alpha \rightarrow t + p + p + \pi^-$	3.3 ± 1.1
$n + \alpha \rightarrow p + p + p + n + n + \pi^-$	1.8 ± 0.8
$n + \alpha \rightarrow$ unclassified $+ \pi^-$	0.6 ± 0.4
Total	100.0

Energy and angular distribution data are presented. A simple phenomenological interpretation of the cross sections is proposed.

PION PRODUCTION BY NEUTRONS ON HELIUM

Peter Hill Moulthrop

Radiation Laboratory, Department of Physics,
University of California, Berkeley, California

January 31, 1955

I INTRODUCTION

Soon after the 184-inch cyclotron was converted to accelerating protons, mesons produced by proton bombardment of carbon were found in photographic emulsions,[1] and mesons were also observed in a cloud chamber[2] placed in the neutron beam. Since then many data on meson production in nucleon-nucleon collisions have been obtained at Berkeley and elsewhere, and a satisfactory phenomenological theory has been evolved.[3] Considerable data are also available on meson production in nucleon bombardment of nuclei, but the theory is fragmentary.

This is an account of an experiment on the production of mesons by 300-Mev neutron bombardment of helium gas contained in a high-pressure diffusion cloud chamber. Considerable advantages inhere in the cloud chamber method in that a pure target is used, mesons of all angles and energies are detected, and measurements can be made on all prongs coming from a star in which a meson originates. As negative mesons predominated over the positives by a large factor and the neutrals can only be detected in rare instances, most of the following is limited to the negative mesons. Attention in this experiment was focused on the following points:

<u>Branching ratio</u>

The various possibilities for producing a negative pion are:

3-prong stars

$$n + \alpha \rightarrow \alpha + p + \pi^-,$$

$$n + \alpha \rightarrow He^3 + d + \pi^-,$$

$$n + \alpha \rightarrow He^3 + p + n + \pi^-.$$

4-prong stars

$$n + \alpha \rightarrow t + p + p + \pi^-,$$
$$n + \alpha \rightarrow d + d + p + \pi^-,$$
$$n + \alpha \rightarrow d + p + p + n + \pi^-,$$
$$n + \alpha \rightarrow p + p + p + n + n + \pi^-$$

The relative yields of these processes were found.

Fast prongs

Large momentum transfers occur between the nucleons involved in meson production. Thus it is of interest to classify the stars as to the most energetic prong ejected; the possibilities are proton, deuteron, triton, He^3, or alpha.

Angular distribution

The angular distribution for meson production in helium is of interest because the lightest saturated nucleus on which large-angle data are available is carbon.

Energy distribution

Kinoshita[4] has indicated that Coulomb distortion of the energy spectrum of the mesons may be serious up to meson energies of 30 Mev for nuclei where the charge is high. Because of the low charge on helium, this distortion becomes significant at lower energies; most of the mesons would not show this distortion.

Numerical values of the cross sections

By use of certain extrapolations, numerical values of the cross sections were obtained.

Rare events

A few rare events were found and are discussed briefly.

The cloud chamber

This experiment served to provide an operational test of the cloud chamber prior to its employment at the bevatron.

II EXPERIMENTAL PROCEDURE

Cyclotron Run

Neutron beam

The beam was produced by 340-Mev protons striking a 1.75-inch LiD target placed inside the Berkeley cyclotron at a radius of 80-7/8 inches. A plan view of this arrangement is shown in Fig. 1. The energy spectrum of the neutrons was measured by De Pangher,[5] and is shown in Fig. 2. The beam passed through a brass collimator 7 feet long with an aperture 4 inches wide by 1 inch high, and then through a hole in the concrete shielding. This collimator had a 12-inch paraffin plug in its exit end to selectively attenuate low-energy neutrons.[*6] The 3-foot copper collimator directly in front of the cloud chamber passed a beam 2.75 inches by 1 inch; the beam entered and left the chamber through 12-mil beryllium-copper windows. A large neutron counter in back of the chamber was used for monitoring the beam.

Photography

Stereoscopic pairs of photographs were taken by an especially constructed camera mounted directly on the cloud chamber 28.5 inches above the sensitive volume. The 50-mm Leitz Summitar lenses, stopped to f/9, viewed the chamber through 1.5-inch-diameter ports backed by 0.75-inch-thick parallel flats of boro-silicate crown glass. A third lens viewed a magnet ammeter and a number counter. The film used was Eastman Linagraph Pan in strips 1.8 inch wide and 400 feet long. The pictures were taken by discharging 256 microfarads charged to 1,700 volts through each of two General Electric flash tubes mounted on either side of the chamber.

Operation cycle

The cycle of operation, repeated every 75 seconds, is as follows: the clearing field is turned off, the magnet current is turned on and a ready signal is sent to the cyclotron, the arc source and radiofrequency system are then turned on for three frequency-modulation cycles, and 0.1 second later a 50-kilovolt pulse initiates the light flash.

---

* We are indebted to Dr. Schluter for a preprint of his article in which this idea is mentioned.

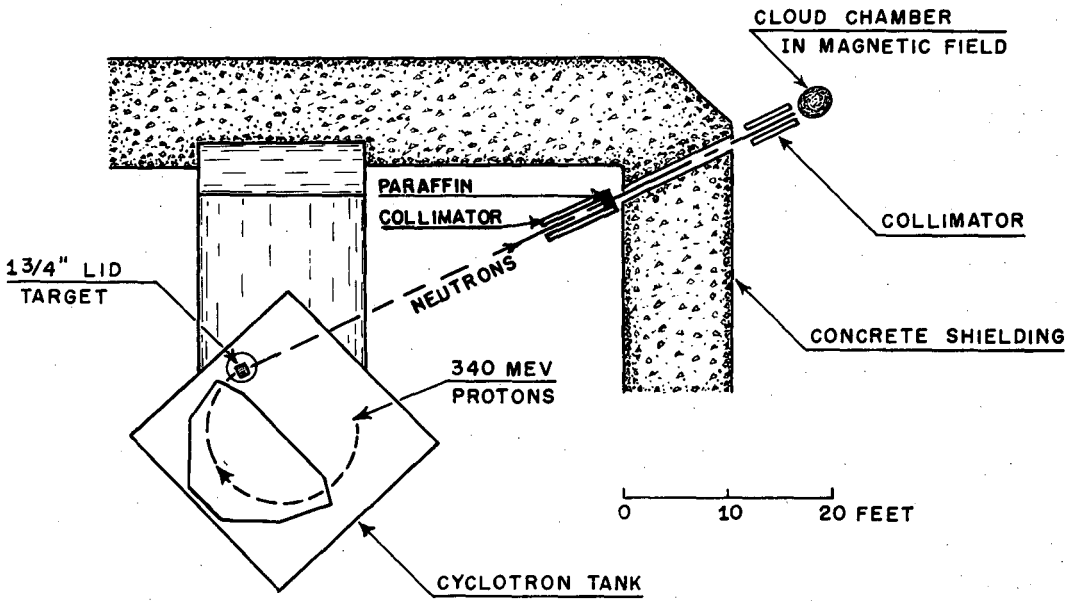

MU-5006-A

Fig. 1 Plan view showing cloud chamber in neutron beam from cyclotron.

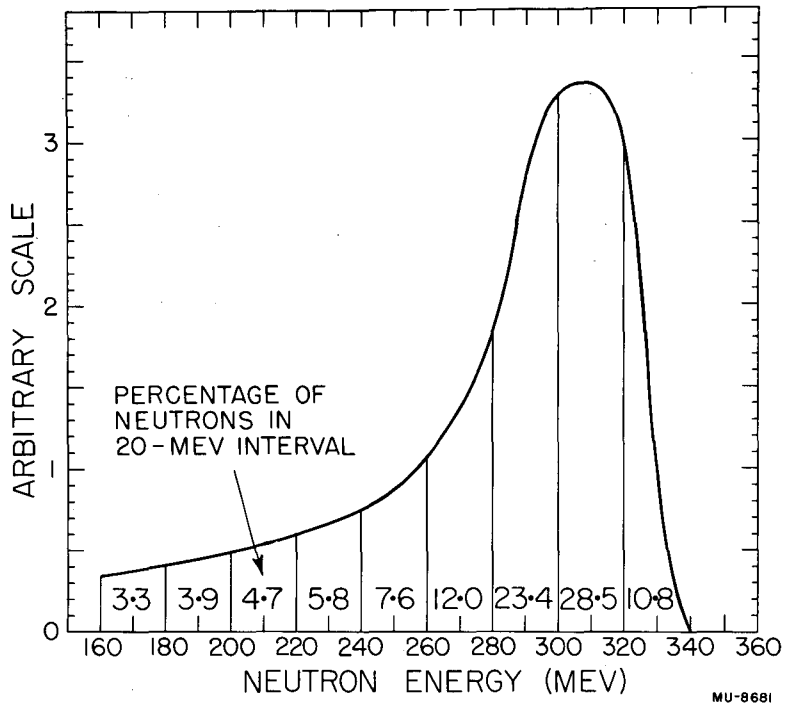

Fig. 2 Neutron energy spectrum as obtained by De Pangher

The Cloud Chamber

The pioneer work on high-pressure diffusion chambers, both in theory[7] and in practice,[8] was carried out by Ralph P. Shutt and collaborators at the Brookhaven National Laboratory; the work at Berkeley proceeded under the stimulus of their success. The present chamber was designed by Wilson M. Powell to fit an existing magnet;[9] a photograph of the chamber is shown in Fig. 3.

The design pressure of this chamber is 525 psi gauge pressure. The experiment reported herein was done at an absolute pressure of 33 atmospheres, with the temperature in the sensitive volume between -10° and -65°C. The nonmagnetic stainless steel base N is welded (R) to a section of hot-rolled steel, F, 9.25 inches above the bottom of the chamber. From the weld up the chamber serves as the top pole of the magnet. Values of the magnetic field at 4,000 amp magnet current for different positions in the chamber are given in Appendix I. Figure 4 shows a quarter-scale cutaway view of the chamber. Water at 33°C was circulated through four squirt tubes, E, in the pole assembly. Acetone at dry-ice temperature was pumped through two parallel paths (O,P) to cool the bottom of the chamber. Reagent-grade methyl alcohol was added to the trays K under gravity feed and drained from the bottom every four hours. Black dye in the alcohol provided an excellent photographic background.

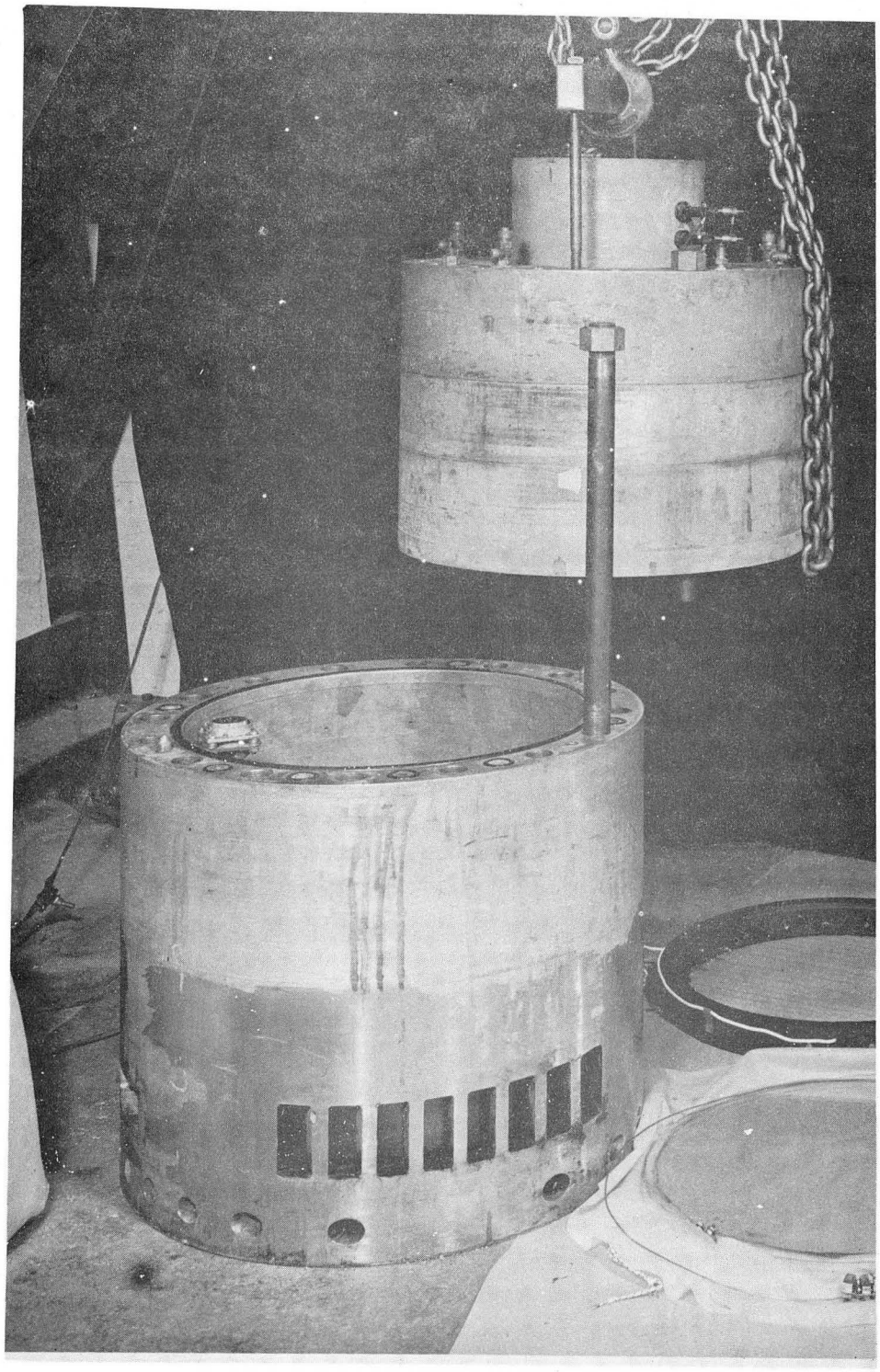

ZN-1175

Fig. 3 The cloud chamber.

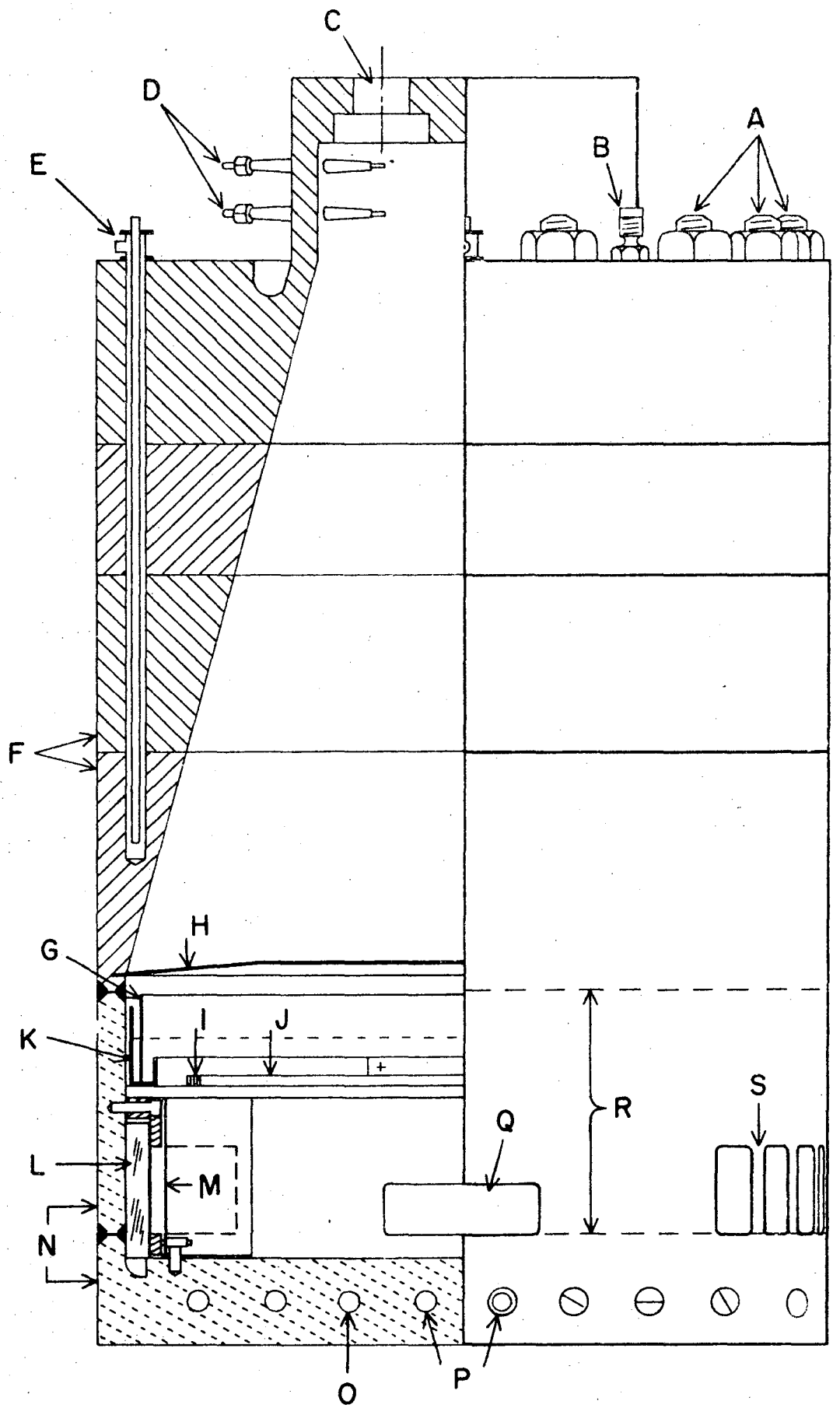

ZN-1186

Fig. 4.

Fig. 4 Quarter-scale cutaway view of the cloud chamber

A Stressproof steel main bolts, 1-by-16 inches (16)

B Pressure line to interior of chamber for gas or alcohol (3)

C Viewing and camera ports (4)

D Spark plugs for clearing field and thermocouples (8); no electric heating is used with this chamber at present

E Squirt tubes (4)

F Upper pole assembly

G Wick

H Black bakelite ring

I Bakelite clearing-field support

J Clearing-field wires (5)

K Copper alcohol tray

L Cast astrolite windows (2)

M Homalite heat shield, 1/16-inch

N Nonmagnetic stainless steel

O Acetone channel

P Acetone inlets (2)

Q Beryllium-copper windows 0.012 x 1.25 x 3 inches (details not shown)

R Welds

S Ribs, 3/4 x 1 inch, to support windows L (7 ribs on each side)

III MEASUREMENTS AND REDUCTION OF OBSERVATIONS

Detection and Measurement of Events

Available data

The information used in the analysis consisted of the film from five days of cyclotron run, a knowledge of the neutron spectrum, mass values for all particles involved, conservation laws for the energy-momentum 4-vector and electric charge, the number of ions produced per cm of path as a function of energy, and range-energy data for the particles involved. Table I lists the Q-values and thresholds for the reactions leading to negative pion production.

Table I

Kinematics of Negative Pion Production in n-α Collisions

Reaction	Q-Value (Mev)	Threshold (Mev)
$n + \alpha \rightarrow \alpha + p + \pi^-$	-138.2	175.5
$n + \alpha \rightarrow He^3 + d + \pi^-$	-156.6	199.0
$n + \alpha \rightarrow He^3 + p + n + \pi^-$	-158.8	201.9
$n + \alpha \rightarrow t + p + p + \pi^-$	-158.0	200.3
$n + \alpha \rightarrow d + d + p + \pi^-$	-162.0	205.8
$n + \alpha \rightarrow d + p + p + n + \pi^-$	-164.3	208.8
$n + \alpha \rightarrow p + p + p + n + n + \pi^-$	-166.5	211.9

Scanning

All film was scanned and rescanned for meson stars and for electron-positron pairs starting in the gas produced by gamma rays from the cyclotron target. The location and identification of mesons usually depended on the facts that they have negative charge and originate from three- or four-prong stars. For sufficiently long tracks mesons can be located and identified by their radius vs ionization. The rescanning usually resulted in less than a 10 % increase in the total number of events found on a particular strip of film. In cases where either the first or the second scanning seemed to have less than a 90% efficiency a third scan was made. In no case did the third scan increase

the event total by more than a few percent. The scanning was done by reprojecting the film on a piece of white cardboard on top of a table at which the scanner was seated. The projector used was a Stereo-Vivid arranged so that individual views could be projected either separately or together. The events found were sketched so they could be relocated later. After scanning, all sections of film on which minimum ionizing tracks were not apparent or which were underdeveloped were discarded.

Reprojection and recording of data

The events were measured on reprojection apparatus similar to that described by Brueckner et al.[10] and shown in Fig. 5; a good description of the method of measuring is given by Fuller.[11] For each event the following information was recorded: film number, height of origin, position in chamber (in a grid coordinate system defined by the clearing-field wires), magnet current, number of prongs. For each track the following information was recorded, as applicable: radius; length or range; apparent track density; dip angle α between the track and its projection on a horizontal plane; beam angle β between the horizontal projection of the track and the beam; height and horizontal distance from the pole centerline of the center of the track (for purposes of determining the field effective on the track).

Identification of Particles

This discussion is conveniently divided into three- and four-prong events.

Three-prong events. The majority of the three-prong events have a fast proton or deuteron and a helium isotope with a range of a few centimeters. The fast prong is identified by comparing track density with near-by proton tracks in the gas; the number of ions produced by deuterons is greater than the number of ions produced by protons at the same radius by a factor of three. A further aid in the identification is that high-momentum fast prongs can only be deuterons, according to conservation of energy. For example, if the meson plus the helium have 40 Mev of kinetic energy, the highest-energy proton possible is

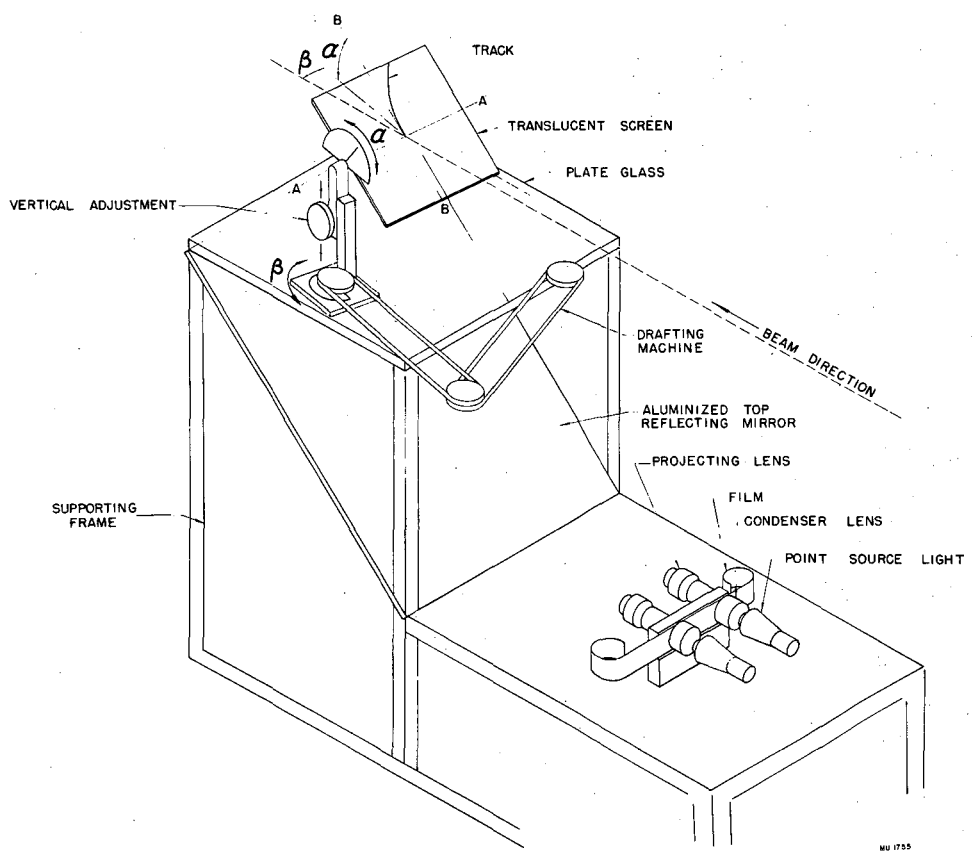

Fig. 5 The stereoscopic projection apparatus.

160 Mev. This has the same $B\rho$ as a deuteron of 85 Mev; thus if the deuteron has over 85 Mev it cannot be mistaken for a proton. A third of the $He^3 + d + \pi^-$ events were unambiguously identified by this criterion. If one fragment is a deuteron, the remaining track must be a He^3. If the fast prong is a proton, the helium isotope can be distinguished when it has a range of several cm, and stops in the gas, by its characteristic ending. On the other hand, for 1- or 2-cm tracks the helium isotopes are indistinguishable. Most of the helium tracks, not identified by track appearance, were identified as He^3 on the basis that (a) the event showed a transverse momentum unbalance outside of experimental error; (b) the assumption that the helium was an alpha led to a calculated incoming-neutron energy below threshold for this process; or (c) the discrepancy in incoming-neutron energy calculated from outgoing energy and outgoing momentum was outside of experimental error. Fourteen out of the 107 events observed remained ambiguous, giving a good fit as either $He^3 + p + n + \pi^-$ or $\alpha + p + \pi^-$.

Four-prong events. Three hydrogen isotopes starting at the same point in the chamber are available. The identification was made by comparing the radii and specific ionizations of these tracks with the possible combinations in mind.

Errors

Remeasurements

Following the measurements an energy-momentum balance was attempted for all events (details of these calculations are illustrated in Appendix II). Thirty percent of the events showed an unbalance outside of experimental error. All these events and 30 "balanced" events selected at random were remeasured and recalculated. Errors in identification, measurements, recording of measurements, or calculations were found to account for the unbalances. Each track involves three measurements, and each event three or four tracks. Of the 30 events which originally balanced one was changed on remeasurement from $He^3 + d + \pi^-$ to $\alpha + p + \pi^-$. The measurements on the remaining 29

events agreed within the expected experimental errors.

Turbulence and optical distortion. The measured apparent radius of minimum ionizing tracks crossing the chamber with the magnetic field turned off is greater than 30 meters; the highest-energy tracks measured in the present experiment had radii of less than 1 1/2 meters. Thus, these errors are small compared to the errors of measurement discussed below.

Radius of curvature. The curvature of a track is measured by reprojecting it life-size on a translucent screen which is rotated in space until it contains the plane of the tracks (called the slant plane), and then matching it with one of a series of arcs ruled on a lucite template. The author's experience in this and previous experiments is that the discrepancies found in attempts to reproduce this measurement amount to 0.1 mm in sagitta. If the radius in the slant plane is called ρ_s, the length L, and the sagitta s, then

$$\rho_s = \frac{L^2}{8_s} \text{ and } \frac{\delta\rho_s}{\rho_s} = \frac{8\rho_s \ \delta_s}{L^2} = 0.08 \ \frac{\rho_s}{L^2} .$$

The pions with dip angle α less than 45° were used for the energy distributions. The quantity $\frac{\delta\rho_s}{\rho_s}$, which is equal to the uncertainty in momentum for small dip angles, has been calculated for the 256 mesons observed in this range of dip angles, with the result shown in Table II.

Table II

Uncertainty in Radius of Curvature for Negative Pions Used in Energy Distributions

$\frac{\delta \rho_s}{\rho_s}$ percent	Number of Pions
0 - 4	129
5 - 9	54
10 - 14	19
15 - 19	19
20 - 24	9
25 - 49	17
50 - 99	8
≥ 100	11

Range-energy relationships

Aron, Hoffman, and Williams[12] give data for helium at 15° C and one atmosphere. The chamber in this experiment was operated at 33 atmospheres and an average temperature of -40°C. This is the same density as 41 atmospheres at 15°C. The vapor pressure of methanol at -40°C is 0.02 atmosphere. A molecule of methanol has 18 electrons; if the chamber is 8-fold supersaturated, the contribution of the methanol is 1.5 atmospheres. Therefore, the ranges in Reference 12 were divided by 42.5. In order to check the range-energy relationship, the energies of a group of long tracks that ended in the chamber were determined by range and by radius measurements. Agreement within 10% was obtained.

Dip angle α and beam angle β

As judged from the reproducibility of measurements, the error in dip angle α is $\pm 1.5^\circ$ for dip angles up to 50°, the error in beam angle β is $\pm 1^\circ$. In this experiment, through oversight, the chamber

was not securely fastened in the magnet and turned through 4° between the time when it was aligned in the neutron beam and the end of the run. A correction for this was effected by measuring the apparent beam angle of electron-positron pairs starting in the gas owing to gamma rays from neutral pions that decayed in the target. This beam angle was taken as the 0° direction. This was plotted as a function of picture number and was used to correct the raw data. Encouraging evidence that this was in fact the right correction was obtained by considering the transverse momentum unbalance in the horizontal direction for those events with no emergent neutron. A plot of transverse unbalance vs number of events centered at zero had a half width at half height of 0.7×10^{5} gauss-cm. The incoming neutron momentum was about 28×10^{5} gauss-cm. If the whole discrepancy were due to an error in angle the error would be about $\pm 0.7/28$ radian or $\pm 1.5^{o}$. A similar result for the vertical unbalance with $\pm 1 \times 10^{5}$ gauss-cm was obtained.

Corrections

Difficulties in observing and aligning mesons with a dip angle greater than $\pm 60^{o}$ led to restricting the measurements to tracks with smaller dip angles. Presumably all events happen with azimuthal symmetry; if this is true a geometrical weighting factor can be applied to all tracks to correct for the excluded regions. Table III lists all mesons observed in four azimuthal groups for which there is no excluded region, and also shows the number of mesons in all azimuthal groups in the forward and backward 60° cones.

Table III

Azimuthal Symmetry Check

Azimuthal Group ϕ	Number of Pions $0^\circ \leqslant \theta \leqslant 180^\circ$	$0^\circ \leqslant \theta \leqslant 60^\circ$	$120^\circ \leqslant \theta \leqslant 180^\circ$
0 - 60	46	23	5
60 - 120		21	4
120 - 180	62	36	9
180 - 240	65	29	7
240 - 300		22	2
300 - 360	66	38	7

This disagreement is not outside that to be expected from statistical fluctuations. A derivation of the geometrical weighting factor is given in Appendix B of Reference 5; if the cutoff dip angle is α_o the formula is

$$(1) \quad f(\alpha_o) = \frac{\pi/2}{\sin^{-1}\left(\sin \alpha_o / \sin \theta\right)}$$

Figure 6 is a plot of Eq. (1). The 60° cutoff was applied to both the angular distribution and the heavy-fragment data; as noted previously a 45° cutoff was used for the energy distributions.

Carbon and oxygen events

In the section on range-energy relationships it was estimated that the methanol-to-helium ratio was about 1:250. If the ratio of the cross sections is 5:1, about six negative mesons from carbon or oxygen should have been observed. Six events attributed to carbon or oxygen were found.

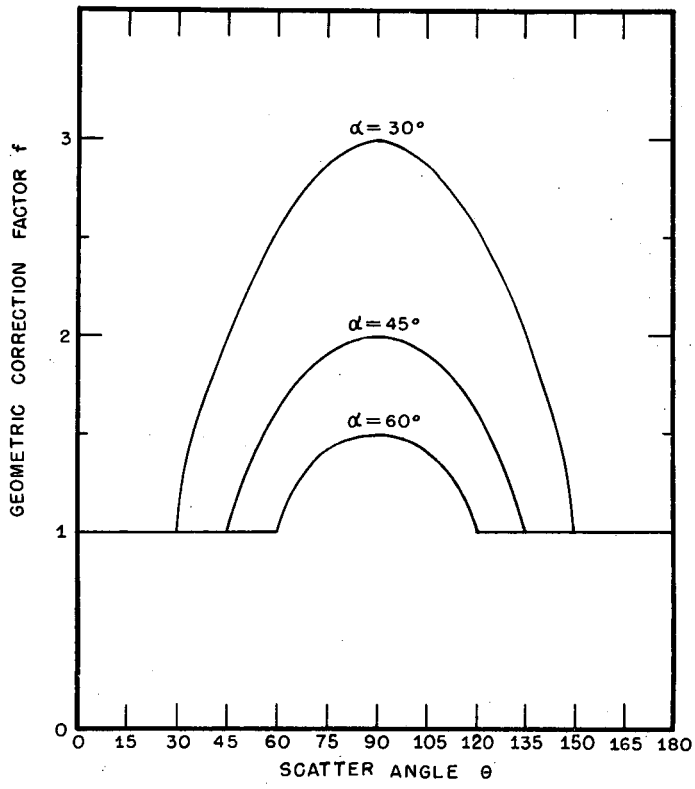

ASSIGN WEIGHT f TO EACH TRACK SEE APPENDIX V

MU-5007

Fig. 6 Geometrical weighting factor.

RESULTS AND DISCUSSION

Branching Ratios and Fast Prongs

Data

Table IV shows the relative yields of the processes leading to negative pion production; uncertainties shown are standard deviations.

Table IV

Relative Cross Sections for Processes Indicated

Reaction	Actual Number Observed	Weighted Number	Percent
$n + \alpha \rightarrow \alpha + p + \pi^-$	17	18.5	5.7 ± 1.4
$n + \alpha \rightarrow He^3 + p + n + \pi^-$	93	104.0	32.0 ± 3.3
$n + \alpha \rightarrow \alpha + p + \pi^-$ or $n + \alpha \rightarrow He^3 + p + n + \pi^-$	14	14.9	4.6 ± 1.2
$n + \alpha \rightarrow He^3 + d + \pi^-$	91	98.9	30.4 ± 3.2
3-prong unclassified	1	1.0	0.3 ± 0.3
$n + \alpha \rightarrow t + p + p + \pi^-$	9	10.8	3.3 ± 1.1
$n + \alpha \rightarrow d + d + p + \pi^-$	18	20.3	6.2 ± 1.5
$n + \alpha \rightarrow d + p + p + n + \pi^-$	46	50.1	15.4 ± 2.3
$n + \alpha \rightarrow p + p + p + n + n + \pi^-$	5	5.8	1.8 ± 0.8
4-prong unclassified	1	1.3	0.3 ± 0.3
totals	295	325.6	100.0

In Table V and Table VI the data are broken down further in terms of the most energetic heavy prong ejected.

Table V

Fast Heavy Prongs Associated with Negative Pion Production

Particles Present in Final State	Weighted Number of Events with Most Energetic Prong as Indicated						
	Proton	Deuteron	Triton	He^3	Alpha	He^3 or Alpha	Total
α, p, π^-	14.1				4.4		18.5
He^3, p, n, π^-	56.8			47.2			104.0
α, p, π^- or He^3, p, n, π^-	12.7					2.2	14.9
He^3, d, π^-		77.1		21.8			98.9
t, p, p, π^-	4.8		6.0				10.8
d, d, p, π^-	10.2	10.1					20.3
d, p, p, n, π^-	30.8	19.3					50.1
p, p, p, n, n, π^-	5.8						5.8
Totals	135.2	106.5	6.0	69.0	4.4	2.2	323.3

Table VI

Fast Heavy Prongs Associated with Negative Pion Production

Particles Present in Final State	Weighted Number of Events with Most Energetic Prong Above 50 Mev as Indicated							
	Proton	Deuteron	Triton	He^3	Alpha	He^3 or Alpha	None	Total
α, p, π^-	12.1				3.4		3.0	18.5
He^3, p, n, π^-	33.9			21.0			49.1	104.0
α, p, π^- or He^3, p, n, π^-	9.7					2.2	3.0	14.9
He^3, d, π^-		56.7		7.7			34.5	98.9
t, p, p, π^-	3.8		2.9				4.1	10.8
d, d, p, π^-	10.2	4.0					6.1	20.3
d, p, p, n, π^-	16.7	9.6					23.8	50.1
p, p, p, n, n, π^-	5.8							5.8
Totals	92.2	70.3	2.9	28.7	3.4	2.2	123.6	323.3

By comparing the results in these tables with other experiments one may seek clues to reaction mechanisms. Variables to be considered are (a) the energy and momentum available to the nucleons in the center-of-mass system; (b) elementary reaction cross sections, e.g., $n + n \rightarrow \pi^- + d$, $n + n \rightarrow \pi^- + n + p$, stripping, and pickup; (c) selection rules due to isotopic spin, and Pauli-principle complications. For convenience the experiments cited are listed here:

1. Tannenwald[13] studied stars formed by 90 Mev-neutron bombardment of helium in a cloud chamber; the final energy available to the nucleons in the present experiment is about 100 Mev. A theory[14] is also available.
2. Knapp[15] observed negative pions from 300-Mev neutron bombardment of deuterium gas.
3. Ford[16] carried out a similar experiment with oxygen gas.

A revealing comparison with Tannenwald's experiment is possible by invoking the principle of charge symmetry and comparing his inelastic cross sections to the cross sections in this experiment for all processes except $\alpha + p + \pi^-$ which is the analog of his elastic process.

Table VII

Partial Cross Sections in Two Experiments. Reactions Identified by Particles Present in Final State

300-Mev $n + \alpha \rightarrow \pi^-$ "inelastic"		90-Mev $n + \alpha$ inelastic	
Reaction	Percent	Reaction	Percent
p, He^3, n, π^-	34 ± 3	p, t, n	45 ± 6
d, He^3, π^-	32 ± 3	d, t	14 ± 3
p, p, d, n, π^-	16 ± 1	p, d, n, n	16 ± 3
d, d, p, π^-	7 ± 1	d, d, n	8 ± 2
p, p, p, n, n, π^-	2 ± 1	p, p, n, n, n	1 ± 1
t, p, p, π^-	4 ± 1	He^3, n, n	17 (assumed)
p, He^3, n, π^- or "elastic"	5 ± 1	total	100
total	100		

$$0.89 \pm 0.03 \leqslant \frac{\sigma_{\text{"inelastic"}}}{\sigma_{\text{total}}} \leqslant 0.94 \pm 0.03 \qquad \frac{\sigma_{\text{inelastic}}}{\sigma_{\text{total}}} = 0.49 \pm 0.07$$

Three conclusions drawn from this comparison are: (a) the alpha particle survives pion production about ten percent of the time; further evidence that an alpha particle sometimes survives pion production is the observance of the reaction $\gamma + \alpha \rightarrow \pi^0 + \alpha$ by Goldwasser[17] at the Illinois betatron; half of the 90-Mev cross section is elastic. (b) A real correlation exists between pion production and fast-deuteron formation, i.e., there are many more fast deuterons than can be attributed to the pickup process; the reason these deuterons mainly fall in Row Two in Table VII is that there is little energy left to break up the He^3. (c) The agreements in the "inelastic" cross sections are striking. The "inelastic" cross sections other than p, He^3, n, π^- and d, He^3, π^- can be interpreted by the same sort of arguments needed to understand the 90-Mev cross sections and are not appreciably influenced by the production of a meson. The experiment described here, Tannenwald, and theory all agree that the complete breakup of the alpha particle only happens about one percent of the time; here one of the nucleons is forced into a P state according to the Pauli principle. It might also be noted that Heidmann's theory[14] predicts a ratio between He^3, n, n and p, t, n which differs from that assumed by Tannenwald. The opposing theoretical ideas are:
(A) Heidmann's assumption that the two final unbound nucleons are in an S state with respect to each other. Then the relative probabilities for like and unlike nucleons are $\frac{1/4}{1/4 + 3/4} \left(\frac{V \text{ singlet}}{V \text{ triplet}}\right)^2$ or about one-tenth; this will be the ratio of the He^3, n, n, and p, t, n cross sections. (B) Tannenwald's assumption was that the incoming neutron interacts with and strips a neutron or a proton off the helium; the ratio of the He^3, n, n and p, t, n cross sections is thus $\frac{\sigma_{np}}{\sigma_{nn}} = \frac{\sigma_{np}}{\sigma_{pp}} = 1/3$.
The situation in this experiment is more similar to theory (A), and indeed the ratio found (one-tenth) is in good agreement with this theory.

More evidence on fast-deuteron formation may be had by comparison with Knapp's and Ford's experiments, with "fast" defined as greater than 50 Mev. This is shown in Table VIII.

Table VIII

Fast Fragments Associated with Negative Pion Production by Neutrons Target Gas (Experimenter)

	Deuterium (Knapp)	Helium (Moulthrop)	Oxygen (Ford)
$\frac{\text{Fast Deuterons}}{\text{Fast Deuterons + Fast Protons}}$	0.5 (estimated)	0.38 ± 0.06	0.31 ± 0.06

Pickup and stripping become more important for heavier targets, thus it appears that stripping subtracts more deuterons from the observed yield than pickup adds.

The yield of fast He^3 particles in this experiment is 29 from 323 events; Knapp found 22 in 310 events.

Angular Distribution

The angular distribution based on 295 negative pions is shown in Table IX and Fig. 7.

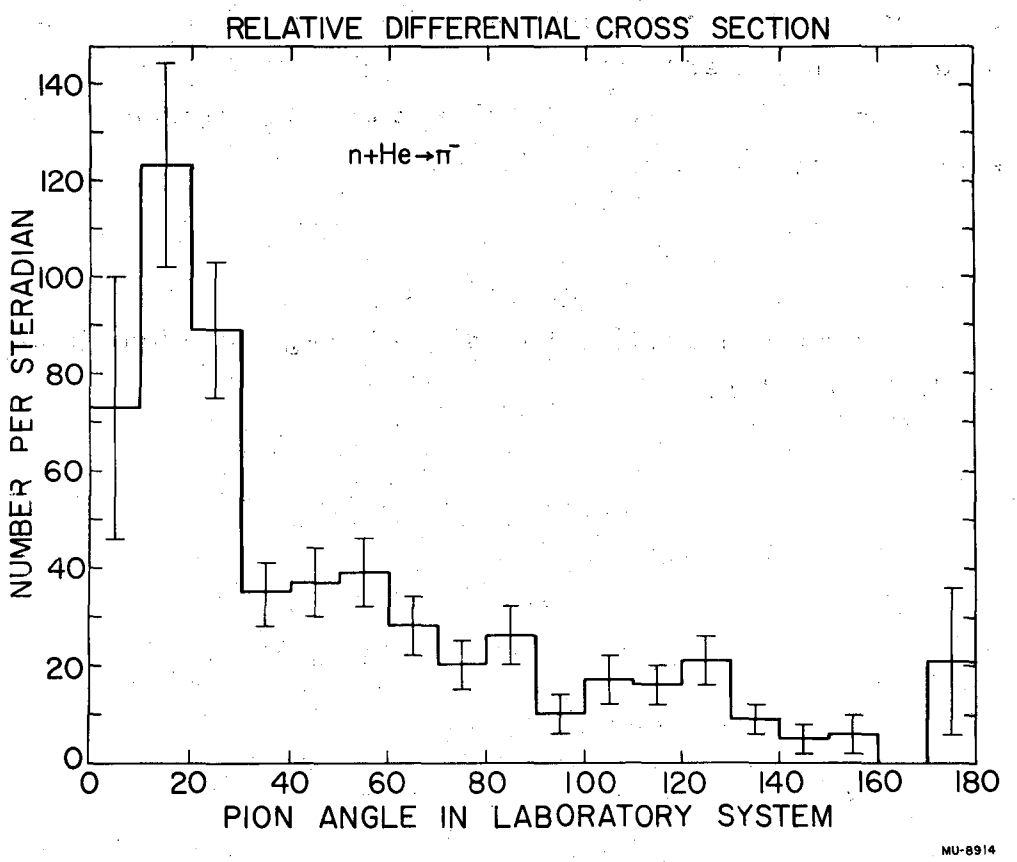

Fig. 7 Angular distribution of pions

Table IX

Relative Differential Cross Sections for Negative Pion Production by 300-Mev Neutrons on Helium

Angular Range θ	Actual Number	Weighted Number	Weighted Number / Unit Solid Angle
0 - 10	7	7.0	73 ± 27
10 - 20	35	35.0	123 ± 21
20 - 30	41	41.0	89 ± 14
30 - 40	22	22.0	35 ± 7
40 - 50	29	29.0	37 ± 7
50 - 60	35	35.0	39 ± 7
60 - 70	24	27.8	28 ± 6
70 - 80	15	21.1	20 ± 5
80 - 90	19	28.5	26 ± 6
90 - 100	7	10.5	10 ± 4
100 - 110	13	18.4	17 ± 5
110 - 120	14	16.3	16 ± 4
120 - 130	19	19.0	21 ± 5
130 - 140	7	7.0	9 ± 3
140 - 150	3	3.0	5 ± 3
150 - 160	3	3.0	6 ± 4
160 - 170	0	0.0	0
170 - 180	2	2.0	21 ± 15

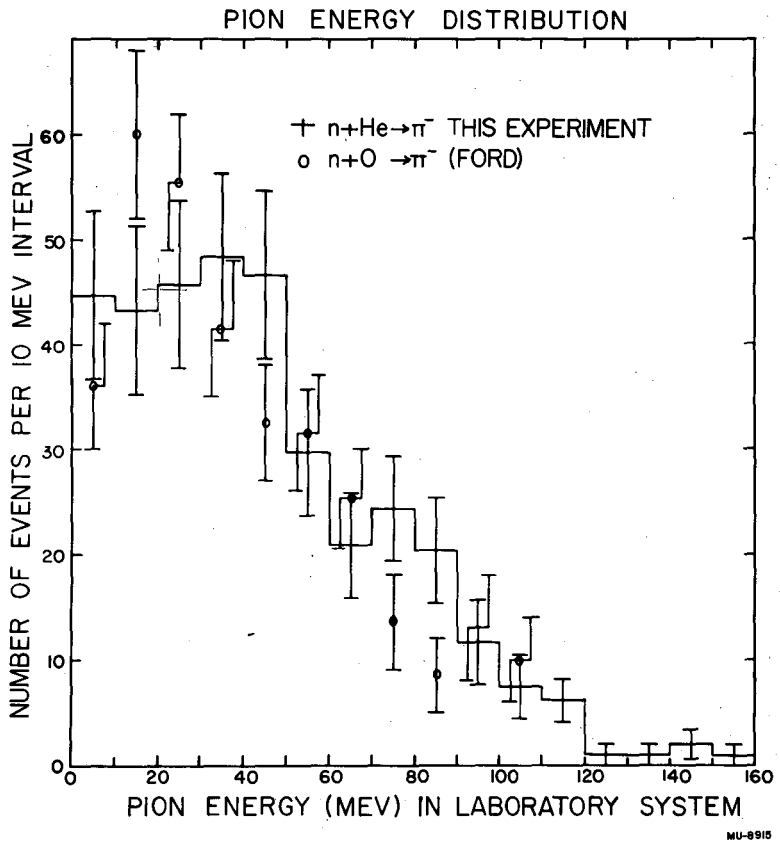

Fig. 8 Energy distribution of all pions.

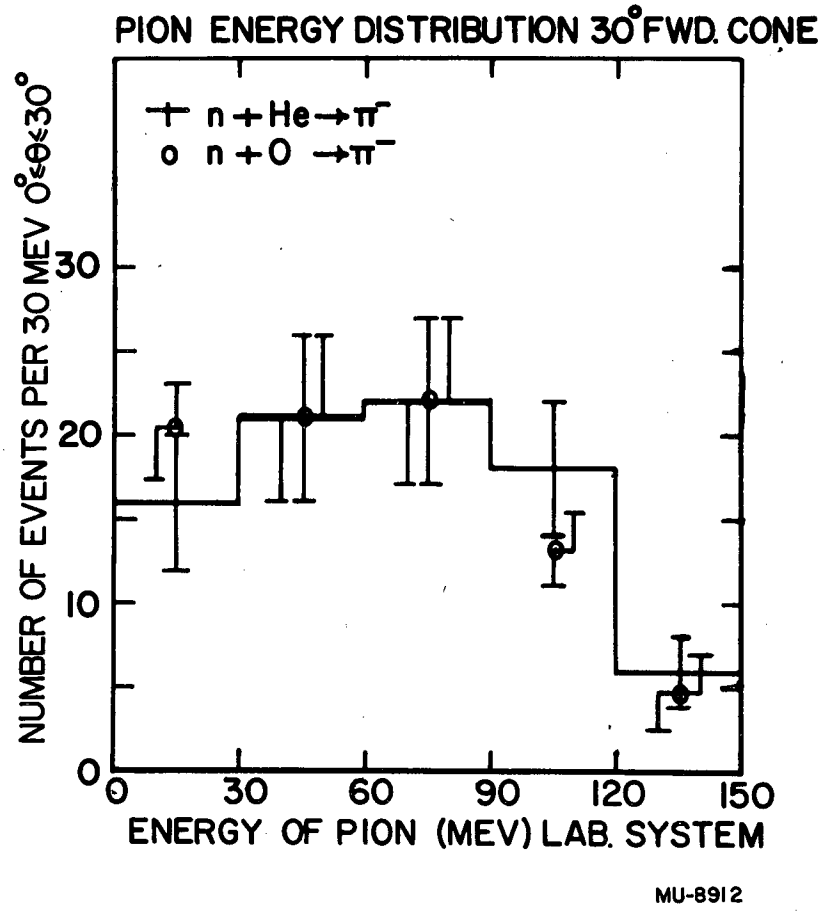

Fig. 9 Energy distribution of pions in 30° forward cone.

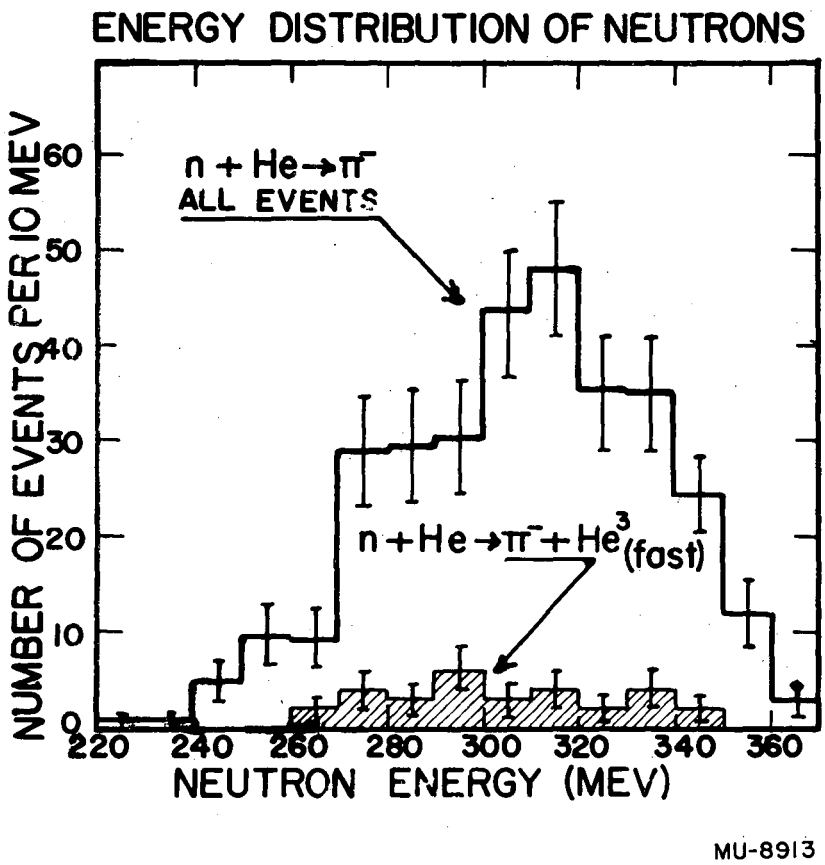

Fig. 10 Energy spectrum of neutrons inducing meson events.

The shape of the angular distribution is in qualitative agreement with all measurements on pion production in nucleon bombardment of nuclei known to the author.[15, 16, 18-20] The gross features are a 0° differential cross section about six times the 90° cross section, and little dependence on angle in the backward hemisphere. Ford and Neher[18] have shown that this shape can be transformed into a nucleon-nucleon average-center-of-mass-system distribution of the form $A + B\cos^2\theta_{cm}$. This procedure is not repeated here.

Energy Distribution

The energy distribution shown in Fig. 8 is also in gross agreement with the results of other experimenters. Ford's results (arbitrary normalization) are plotted in the same figure. The conclusion drawn from the comparison is that the momentum distributions of the nucleons in helium and oxygen are similar. Figure 9 compares the energy spectrum of mesons in a 30° forward cone with those in Ford's experiment.

Energy Spectrum of Neutrons Producting Mesons

Figure 10 is a histogram of incoming neutron energy calculated by the method of Appendix II for those neutrons which produce negative pions (in the rare cases where there are two outgoing neutrons only a lower limit can be set). Comparison with Fig. 2 (the De Pangher spectrum) shows more neutrons in this experiment near 340 Mev, the maximum available in the beam; this is indicative of the steep excitation function for meson production. Knapp found the neutrons inducing $n + d \rightarrow \pi^- + He^3$ to have a lower energy than the other neutrons in his experiment; the neutrons inducing events with a fast He^3 in the present experiment are shown crosshatched on the main histogram. There is no evidence that these neutrons are of lower energy in this experiment.

Total Cross Section

With the assumption of an $A^{2/3}$ dependence, a straight-line extrapolation of Ball's measurements[21] of the inelastic cross sections

for 300-Mev neutrons on Pb, Cu, Al, and C targets give $\sigma_{inelastic} = 70 \pm 10$ mb for helium. The high binding energy in helium may reduce the inelastic cross section below the extrapolated value. The ratio of inelastic two-prong helium stars to meson stars in this experiment was about 120 to 1. Two compensating corrections need to be applied to this ratio: (a) the He^3 one-prong stars are not counted; (b) some of the stars are caused by low-energy neutrons. The final result obtained is $\sigma(n + \alpha \rightarrow \pi^- = 0.6 \pm 0.3$ mb, where the error is estimated on the basis of the many uncertainties present.

Infrequent Events

Positive Pions

As discussed in the section on identification, positive pions are detected with reduced efficiency; it is believed, however, that a positive pion of track length greater than 10 cm could not escape detections; four such positive pions were found while 66 negative pions had over 10 cm visible. This leads to a minus-plus ratio of 16 ± 8. Ford reports a minus-plus ratio of 16.4 ± 3.7 for neutrons on oxygen, and Dudziak[19] estimates a plus-minus ratio of 14 ± 4 for protons on carbon.

Neutral Pions

Charge-independence theory predicts

$$\sigma(n + p \rightarrow \pi^0 + d) = 1/2\ \sigma(n + n \rightarrow \pi^- + d);$$

the current phenomenological theory[3] also yields

$$\sigma(n + p \rightarrow \pi^0 + \text{NUCLEONS}) = 1/2\ \sigma(n + n \rightarrow \pi^- + \text{NUCLEONS})$$

near threshold. The other pion-production cross sections are small. On this basis, corresponding to the 325 negative pions produced in the experiment here described, we expect 160 neutral pions; the two decay modes of the neutral pion,

$$\text{(a)}\quad \pi^0 \rightarrow \gamma + e^+ + e^-,$$

$$\text{(b)}\quad \pi^0 \rightarrow 2\gamma,$$

occur in the ratio 1 to 80.[22,23] Thus we should observe in the cloud chamber two cases of electron-positron pairs originating from helium

stars; two such events were observed and an example is shown in Appendix II. Neutral-pion production in which the decay is by (b) is unobservable in this experiment.

Negative Meson Endings

Five negative pions ended in the chamber and resulted in characteristic one-prong stars; one negative muon ended in a 40-Mev decay electron.

Triplet Production

Figure 11 (event 15841) is a picture of triplet production in the gas, $\gamma + e^- \rightarrow e^+ + e^- + e^-$.

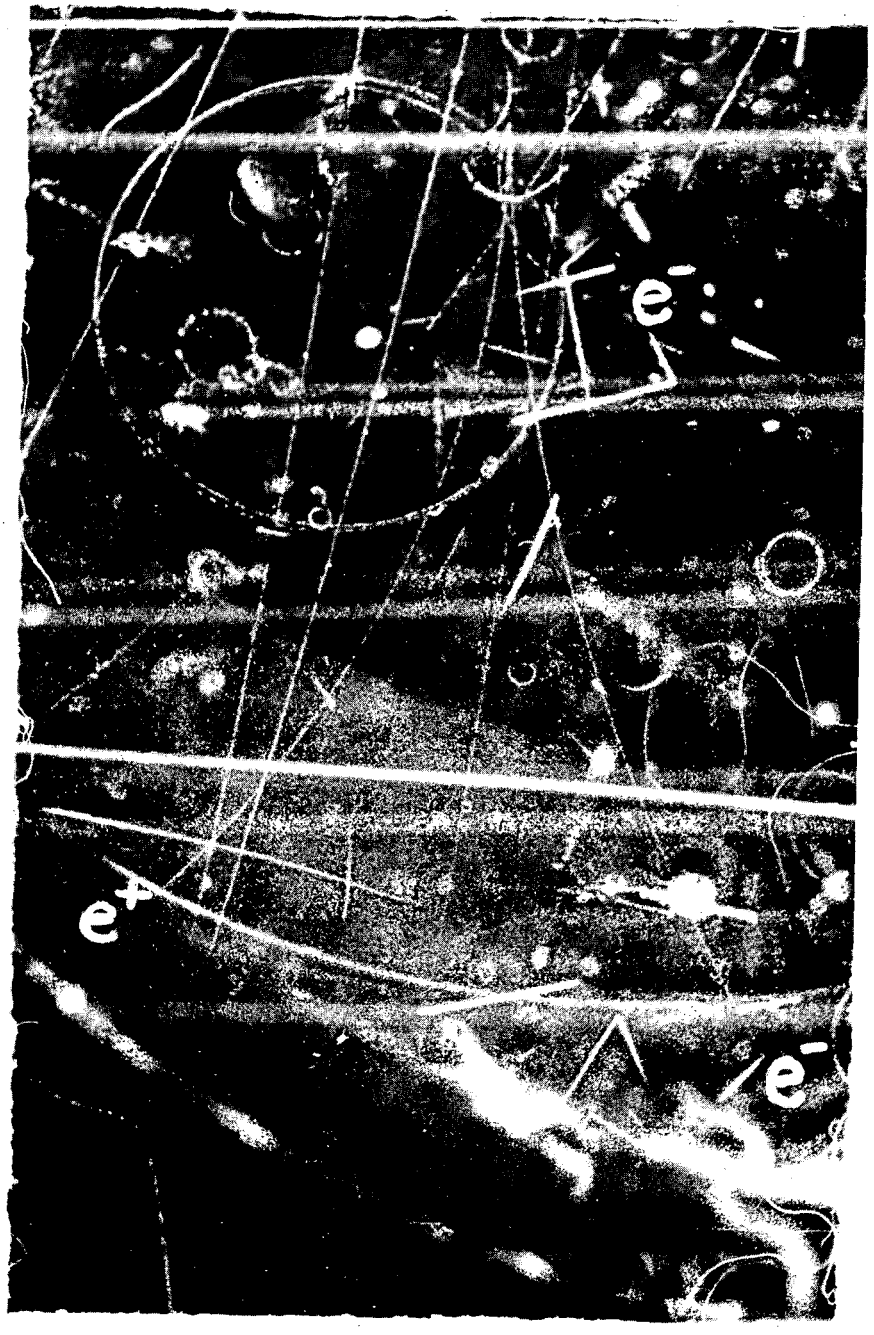

ZN-1155

Fig. 11 $\gamma + e^- \rightarrow e^+ + e^- + e^-$

ACKNOWLEDGMENTS

It is a great pleasure to record the advice, encouragement, and aid received from Professor Wilson M. Powell throughout the course of this experiment.

Among those whose diligence and ingenuity rendered the gestation of the cloud chamber successful are John B. Elliott, Dr. Franklin C. Ford, George Maenchen, Larry O. Oswald, and Robert W. Wright.

Complete cooperation was given by many departments in the Radiation Laboratory and by commercial suppliers on the many problems that arose during the chamber development.

Drs. Myron W. Knapp, George Saphir, and others generously gave of their time to make the cyclotron runs a success.

Miss Barbara Schultz ably assisted with the calculations, and with the preparation of this manuscript.

This research was performed under the auspices of the U.S. Atomic Energy Commission.

Magnetic Field 35 Atm Cloud Chamber 4000 amps File 15,801 (Mag Group)

inches from pole center line

inches above chamber bottom	0	½	1	1½	2	2½	3	3½	4	4½	5	5½	6	6½	7	
0.5	22.22	22.21	22.19	22.17	22.12	22.05	21.99	21.90	21.78	21.64	21.49	21.29	21.40	20.76	20.44	0.5
0.6	22.17	22.14	22.12	22.10	22.05	22.00	21.94	21.84	21.74	21.60	21.44	21.24	21.00	20.73	20.42	0.6
0.7	22.12	22.10	22.08	22.05	22.00	21.97	21.90	21.80	21.69	21.56	21.40	21.20	20.96	20.69	20.38	0.7
0.8	22.05	22.02	22.00	21.99	21.94	21.90	21.82	21.74	21.64	21.51	21.36	21.16	20.91	20.64	20.33	0.8
0.9	22.00	21.99	21.97	21.94	21.90	21.84	21.78	21.69	21.58	21.44	21.31	21.11	20.89	20.60	20.29	0.9
1.0	21.94	21.92	21.90	21.88	21.82	21.78	21.71	21.62	21.53	21.40	21.27	21.07	20.84	20.56	20.24	1.0
1.1	21.88	21.84	21.82	21.80	21.76	21.71	21.64	21.56	21.47	21.36	21.22	21.02	20.80	20.51	20.20	1.1
1.2	21.82	21.80	21.78	21.76	21.71	21.67	21.60	21.51	21.42	21.31	21.18	20.98	20.75	20.47	20.16	1.2
1.3	21.76	21.74	21.71	21.69	21.64	21.60	21.53	21.47	21.38	21.27	21.13	20.93	20.71	20.42	20.11	1.3
1.4	21.71	21.69	21.67	21.65	21.60	21.56	21.49	21.40	21.31	21.20	21.07	20.89	20.67	20.38	20.07	1.4
1.5	21.64	21.62	21.60	21.58	21.56	21.51	21.44	21.36	21.27	21.16	21.02	20.84	20.62	20.33	20.02	1.5
1.6	21.60	21.58	21.56	21.53	21.49	21.44	21.38	21.29	21.20	21.09	20.96	20.78	20.58	20.29	19.96	1.6
1.7	21.53	21.51	21.50	21.48	21.44	21.40	21.33	21.24	21.16	21.04	20.91	20.73	20.53	20.24	19.91	1.7
1.8	21.49	21.48	21.44	21.42	21.38	21.33	21.28	21.18	21.09	20.98	20.84	20.67	20.47	20.20	19.87	1.8
1.9	21.46	21.43	21.40	21.38	21.33	21.29	21.22	21.13	21.04	20.93	20.80	20.62	20.42	20.15	19.82	1.9
2.0	21.40	21.39	21.36	21.33	21.29	21.24	21.18	21.09	20.98	20.88	20.73	20.56	20.36	20.11	19.80	2.0
2.1	21.37	21.33	21.31	21.29	21.24	21.20	21.13	21.04	20.93	20.82	20.69	20.51	20.31	20.07	19.76	2.1
2.2	21.29	21.28	21.24	21.22	21.18	21.13	21.09	21.00	20.89	20.78	20.64	20.47	20.27	20.04	19.73	2.2
2.3	21.24	21.22	21.20	21.18	21.13	21.09	21.02	20.93	20.84	20.73	20.60	20.42	20.22	20.00	19.71	2.3
2.4	21.20	21.18	21.16	21.13	21.09	21.04	20.98	20.89	20.80	20.69	20.56	20.38	20.18	19.98	19.69	2.4
2.5	21.16	21.13	21.11	21.09	21.04	21.00	20.93	20.84	20.76	20.64	20.51	20.33	20.13	19.93	19.64	2.5
2.6	21.11	21.09	21.07	21.04	21.02	20.98	20.91	20.82	20.73	20.62	20.49	20.31	20.11	19.93	19.64	2.6
2.7	21.07	21.04	21.02	21.00	20.98	20.93	20.89	20.80	20.71	20.60	20.47	20.29	20.09	19.91	19.64	2.7
2.8	21.02	21.00	20.98	20.96	20.93	20.89	20.84	20.78	20.69	20.58	20.44	20.29	20.09	19.91	19.64	2.8
2.9	20.98	20.96	20.93	20.91	20.89	20.84	20.80	20.73	20.64	20.56	20.44	20.29	20.09	19.89	19.64	2.9
3.0	20.93	20.91	20.89	20.87	20.84	20.80	20.76	20.69	20.62	20.53	20.42	20.29	20.09	19.89	19.64	3.0
3.1	20.89	20.87	20.84	20.82	20.80	20.76	20.71	20.67	20.58	20.49	20.40	20.27	20.07	19.89	19.64	3.1
3.2	20.84	20.84	20.82	20.80	20.76	20.71	20.67	20.62	20.56	20.47	20.36	20.27	20.07	19.87	19.64	3.2
3.3	20.80	20.80	20.78	20.76	20.73	20.69	20.62	20.58	20.51	20.42	20.33	20.22	20.07	19.87	19.64	3.3
3.4	20.76	20.76	20.73	20.71	20.69	20.64	20.60	20.53	20.47	20.38	20.29	20.20	20.07	19.87	19.67	3.4
3.5	20.71	20.71	20.69	20.67	20.64	20.60	20.56	20.51	20.44	20.36	20.27	20.18	20.04	19.87	19.67	3.5
	0	½	1	1½	2	2½	3	3½	4	4½	5	5½	6	6½	7	

Radial Distance------- field in Kilogauss

PHM & JE 9-21-54

Appendix I

ZN-1176

APPENDIX II

In this appendix are collected some sample pictures and calculations.

I. Event 45622: $n + \alpha \rightarrow \alpha + p + \pi^-$ (shown in Fig. 12)

This event illustrates (1) an unambigously identified alpha particle, and (2) the energy-momentum balance for an event with no outgoing neutron. A tracing of a He^3 ending in the gas showed definitely more curvature than this alpha particle.

Particle	Energy (Mev)	Forward Momentum (gauss-cm)	Vertical Momentum (gauss-cm)	Horizontal Momentum (gauss-cm)
alpha	37.5	$+17.28 \times 10^5$	0×10^5	-0.62×10^5
proton	4.6	$+ 2.87 \times 10^5$	-0.22×10^5	-1.15×10^5
pion	158.0	$+ 8.56 \times 10^5$	$+0.15 \times 10^5$	$+1.66 \times 10^5$
sum	200.1	$+29.25 \times 10^5$	-0.07×10^5	-0.11×10^5

From outgoing momentum the energy of the incoming neutron is 347 Mev; from outgoing energy the incoming neutron energy is 338 Mev; the transverse unbalance is very small.

2. Event 45738B: $n + \alpha \rightarrow He^3 + p + n + \pi^-$ (Fig. 13)

This event shows a tremendous vertical unbalance, which proves there was an outgoing neutrons.

Particle	Energy (Mev)	Forward Momentum (gauss-cm)	Vertical Momentum (gauss-cm)	Horizontal Momentum (gauss-cm)
He^3	73.8	$+19.70 \times 10^5$	$+8.80 \times 10^5$	-1.72×10^5
proton	20.4	$+ 4.62 \times 10^5$	$+2.16 \times 10^5$	$+4.24 \times 10^5$
pion	6.2	$+ 0.33 \times 10^5$	$+0.12 \times 10^5$	-1.36×10^5
sum of visible prongs	100.9	$+24.65 \times 10^5$	$+11.08 \times 10^5$	$+1.16 \times 10^5$
neutron (assumed)	63.5	$+ 3.3 \times 10^5$	-11.1×10^5	-1.2×10^5
grand sum	164.4	27.9×10^5	0×10^5	0×10^5
		Q value 158.8 Mev		

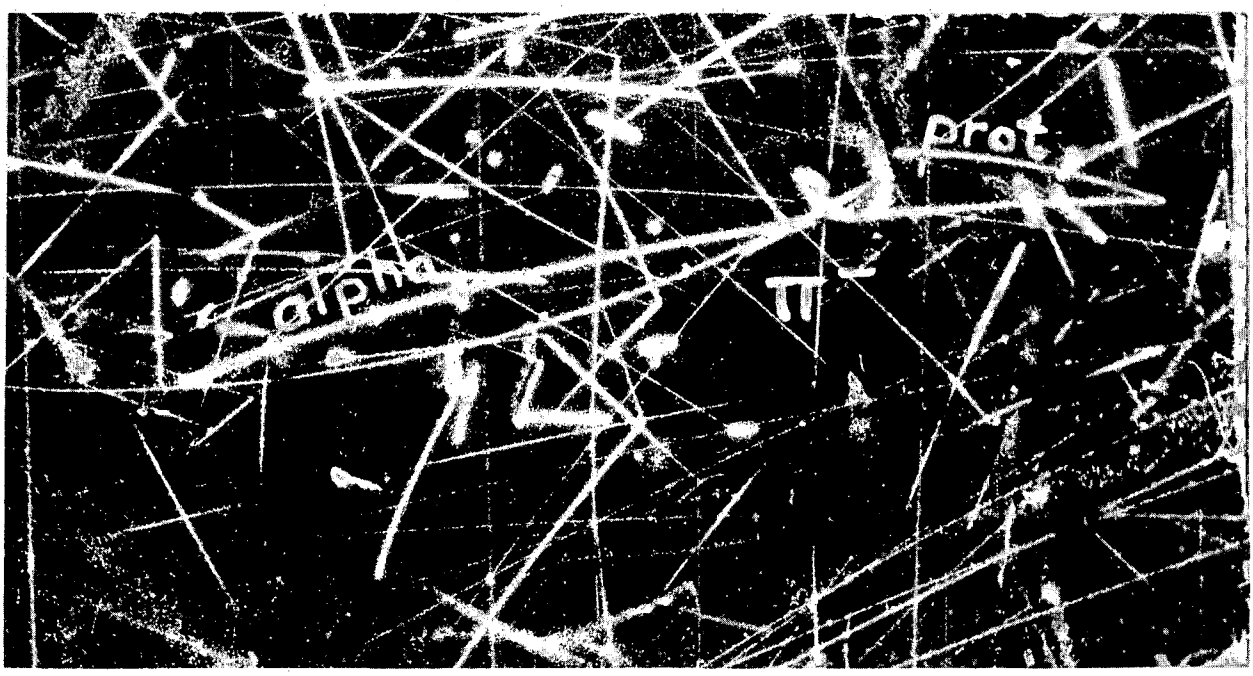

ZN-1153

Fig. 12 $n + \alpha \rightarrow \alpha + p + \pi^-$

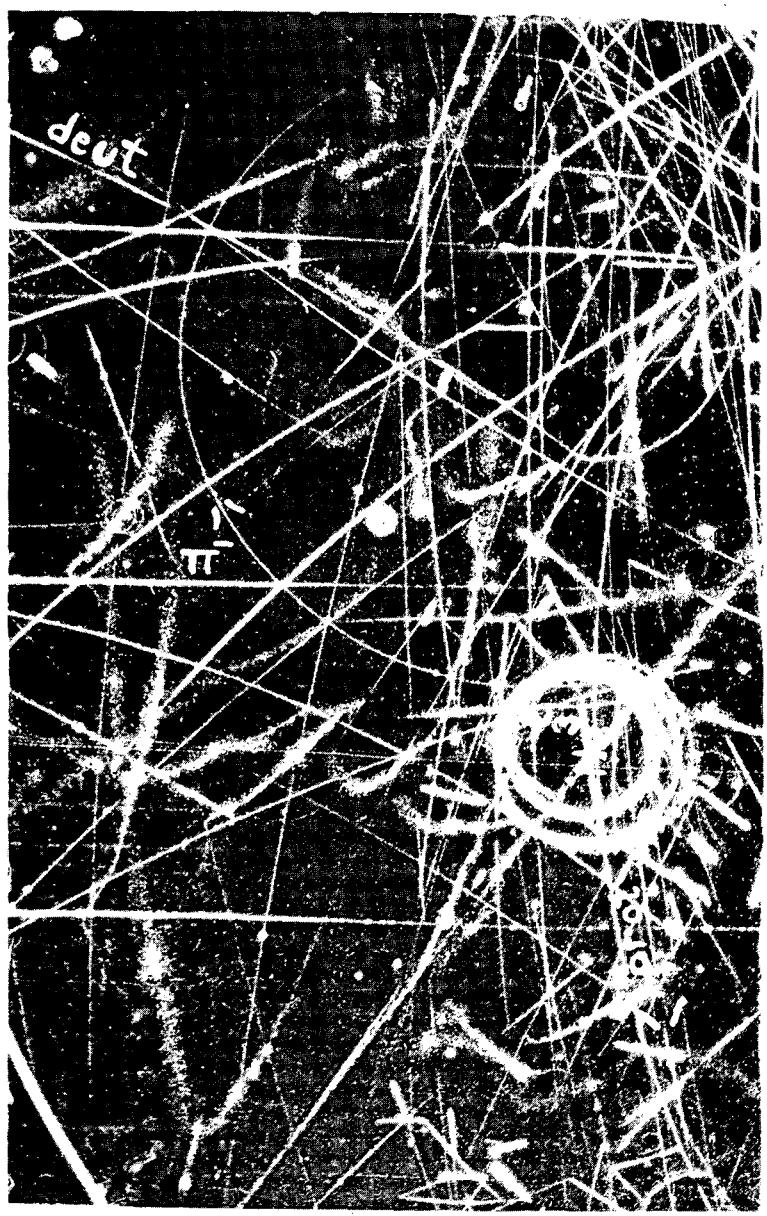

ZN-1156

Fig. 13 $n + d \rightarrow \pi^- + He^3 + p + n$
$\pi^- + \alpha \rightarrow d + 2n$

From outgoing momentum the energy of the incoming neutron is 320 Mev; from outgoing energy the incoming neutron energy is 323 Mev.

Figure 14 shows an electron pair from the reaction $\pi^o \rightarrow \gamma + e^+ + e^-$.

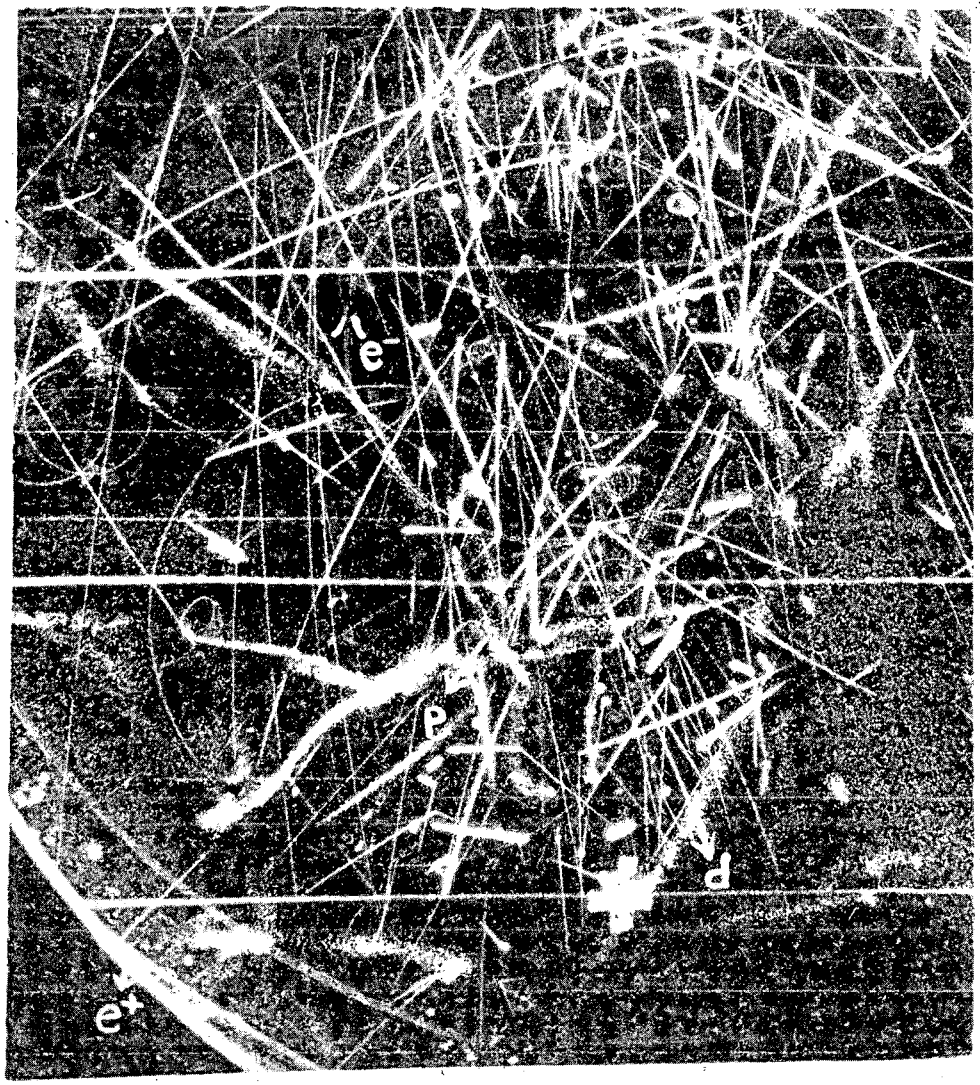

ZN-1154

Fig. 14 $n + a \rightarrow \pi^o + d + p + 2n$
$\pi^o \rightarrow e^+ + e^- + \gamma$

BIBLIOGRAPHY

1. C. Richman and H. A. Wilcox, Phys. Rev. 78, 496 (1950).
2. W. Hartsough, E. Hayward, and W. Powell, Phys. Rev. 75, 905 (1949).
3. A. H. Rosenfeld, Phys. Rev. 96, 139 (1954).
4. T. Kinoshita, Phys. Rev. 94, 1331 (1954).
5. J. De Pangher, Phys. Rev. 95, 578 (1954). See also John De Pangher Jr., A High-Pressure Cloud-Chamber Investigation of Protons Scattered by 300- Mev Neutrons, University of California Radiation Laboratory Report No. UCRL-2153, March, 1953.
6. R. A. Schluter, Phys. Rev. 96, 734 (1954).
7. R. P. Shutt, Rev. Sci. Instr. 22, 730 (1951)
8. R. P. Shutt, E. C. Fowler, D. H. Miller, A. M. Thorndike, and W. B. Fowler, Phys. Rev 84, 1247 (1951).
9. W. M. Powell, Rev. Sci. Instr. 20, 403 (1949).
10. K. Brueckner, W. Hartsough, E. Hayward, and W. Powell, Phys. Rev. 75, 555 (1949)
11. Melvin O. Fuller, Disintegration of Oxygen by 300-Mev Neutrons, University of California Radiation Laboratory Report No. UCRL-2699, September, 1954.
12. W. A. Aron, B. G. Hoffman, and F. C. Williams, "Range-Energy Curves", University of California Radiation Laboratory Report No. UCRL-121, 1949.
13. P. E. Tannenwald, Phys. Rev. 89, 508 (1953).
14. J. Heidmann, Phil. Mag. 41, 444 (1950).
15. Myron W. Knapp, Negative Pions from Neutron Bombardment of Deuterons, University of California Radiation Laboratory Report No. UCRL-2799, November, 1954.
16. Franklin C Ford, The Production of Charged Pi Mesons by Neutrons on Oxygen, University of California Radiation Laboratory Report No. UCRL-2148, March, 1953.
17. E. L. Goldwasser, L. J. Koester Jr., and F. E. Mills, Phys. Rev. 95, 1692 (1954).
18. Leland K. Neher, Meson Production by High-Energy Neutrons, University of California Radiation Laboratory Report No. UCRL-2191, April, 1953.
19. W. Dudziak, Phys. Rev. 95, 866 (1954).

20. S. Leonard, Phys. Rev. 93, 1380 (1954).

21. William P. Ball, Nuclear Scattering of 300-Mev Neutrons, University of California Radiation Laboratory Report No. UCRL-1938, August, 1952.

22. Lindenfeld, Sachs, and Steinberger, Phys. Rev. 89, 531 (1953).

23. B.M. Anand, Proc. Roy. Soc. A, 220, 183 (1953).